Journal of Energy Storage 166 (2026) 122402

Contents lists available at ScienceDirect

Journal of Energy Storage

journal homepage: www.elsevier.com/locate/est

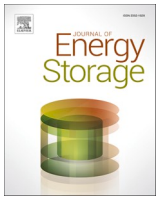

Research Papers

Temperature-dependent electrochemical dynamics in zinc-bromine flow batteries

Jiayi Li, Wenjun Liu, Yongzi Chen, Maochun Wu *

Department of Mechanical Engineering, The Hong Kong Polytechnic University, Hung Hom, Kowloon, Hong Kong

ARTICLE INFO

Keywords:
Zinc-bromine flow batteries
Thermal effect
Polybromide droplets
Oil-water two-phase flow
Zinc deposition

ABSTRACT

Zinc-bromine flow batteries (ZBFBs) are a promising technology for large-scale energy storage, yet the influence of operating temperature on their electrochemical performance and long-term stability remains poorly understood. In this study, we present a systematic investigation of the temperature-dependent behavior of ZBFBs across a wide temperature range. Results show that elevating the operating temperature from 30 to 70 °C significantly improves voltage efficiency from 76.6% to 83.7% at 80 mA cm^{-2} due to reduced polarization. However, this gain is offset by a decline in coulombic efficiency, which decreases from 99.3% to 95.3% as a result of increased bromine crossover and side reactions. Notably, when operated at 50 °C, the ZBFB exhibits the best cycling stability exceeding 1000 cycles due to rapid polybromide/bromide reaction kinetics and uniform zinc deposition. *In situ* optical monitoring and *ex situ* characterizations reveal that below 50 °C, poor mixing of polybromide and localized zinc accumulation near the membrane side lead to shortened cycle life, while above 50 °C, weakened bromine complexation and coarser zinc morphologies accelerate self-discharge and capacity decay. This study provides a comprehensive and mechanistically grounded understanding of how temperature simultaneously influences reaction kinetics, oil-water two-phase flow behavior, zinc deposition and parasitic side reactions, thereby affecting the overall battery performance and offering critical insights for the design of thermally adaptive and long-life ZBFB systems for next-generation energy storage.

1. Introduction

The rapid expansion of renewable energy generation has positioned grid-scale energy storage as a critical technology for enabling reliable utilization of intermittent power from solar and wind [1–3]. Among various energy storage solutions, redox flow batteries (RFBs) are distinguished by their high energy efficiency, high safety, and excellent scalability, making them highly attractive for grid-scale applications [4,5]. In particular, zinc-bromine flow batteries (ZBFBs) have gained increasing attention due to their relatively high energy density, high cell voltage, and the use of low-cost, abundant materials [6–8]. Over the past decades, substantial progress has been made in ZBFBs, with several kilowatt-scale pilot plants successfully demonstrated, showcasing their great potential for practical applications [9–12]. Under real-world operating conditions, ZBFBs are inevitably exposed to significant temperature fluctuations due to geographic and seasonal variations, as well as heat generation during operation [13,14]. These temperature variations can exert a pronounced effect on the physicochemical properties of the electrolytes and the kinetics of electrochemical processes, thereby affecting overall battery performance, including efficiency and cycle life [15,16].

The significance of temperature effects has been well documented in other RFB systems. Most studies have focused on the influence of operating temperature on the performance of all-vanadium RFBs (VRFBs), which represent the most mature flow battery technology [17]. Zhang et al. [15] reported that increasing temperature enhances the voltage efficiency (VE) and peak power density due to enhanced kinetics and reduced ohmic resistance. However, the coulombic efficiency (CE) decreases because higher temperature increases the permeability of vanadium ions through the membrane. Moreover, elevated operating temperature may accelerate the capacity decay rate of VRFBs. Rao et al. [18] first experimentally investigated the sensitivity of the performance of VRFBs to low operating temperature, and showed that optimizing electrode parameters can improve the low-temperature performance. They then developed a physics-based electrochemical model to predict the battery system performance under various operating and climatic environments [19]. Recently, Ren et al. [20] systematically studied the thermal effects on the performance of stack-level VRFBs. It was found

* Corresponding author.
E-mail address: maochun.wu@polyu.edu.hk (M. Wu).

https://doi.org/10.1016/j.est.2026.122402
Received 5 January 2026; Received in revised form 9 April 2026; Accepted 22 April 2026
Available online 28 April 2026

that temperature has a stronger impact on discharge capacity than on efficiency, and optimal operation was achieved at 40 °C and a critical flow rate of 2.88 mL min^{-1} cm^{-2}. The effects of temperature on emerging RFBs have also been explored. For example, Cheng et al. [21] studied the performance and polarization distribution of zinc-nickel single flow batteries ranging from 0 to 40 °C. It was found that the overpotential of the positive electrode during charging is more sensitive to temperature changes. In all-iron RFBs, raising the operating temperature to 60 °C reduced the plating potential and enhanced reaction kinetics of iron deposition, thus improving CE [22].

Unlike the aforementioned RFBs, ZBFBs present unique operational characteristics, involving polybromide oily phase formation/dissolution at the positive electrode and zinc metal plating/stripping at the negative electrode [23,24]. These processes are highly sensitive to temperature variations. In addition to the Br_2/Br^- reaction kinetics, temperature can influence the formation, coalescence, movement and dissolution of polybromide droplets by altering their viscosity, interfacial tension, and density. This, in turn, determines whether bromine is sequestered in the electrolyte or diffuses across the membrane, directly affecting self-discharge performance [25,26]. On the negative side, temperature affects zinc nucleation and growth, thereby controlling the morphology and distribution of zinc deposition [23]. Previous studies revealed that lower temperatures tend to produce denser zinc deposits, while excessively high temperatures induce severe dendrite formation and accelerated zinc corrosion, leading to short-circuits and reduced cycle life of zinc-based flow batteries [27,28]. In addition, Li et al. [25] designed a new bromine complexing agent (1-ethyl-2-methyl-pyridinium bromide) and demonstrated that it enabled ZBFBs to stably operate up to 60 °C. Wang [14] developed a bi-layer graphite felt positive electrode for ZBFBs to improve the Br_2/Br^- reaction kinetics and mass transport. He also found that the ZBFBs equipped with the developed electrodes performed best at 40 °C. Although these studies have shown that temperature can strongly influence the performance of ZBFBs, they have mainly focused on improving individual components or extending operability under selected conditions, whereas how operating temperature affects the underlying electrochemical process and overall performance in ZBFBs remains elusive.

Herein, we present a systematic investigation of temperature-dependent electrochemical dynamics over a broad temperature range (30–70 °C). By separately examining the roles of the positive electrode, negative electrode, and across-membrane transport behavior, this study provides a clearer mechanistic understanding of how temperature governs overall ZBFB performance and cycling stability. It is revealed that operating temperature exerts a pronounced influence on VE, CE, maximum operating current density, and cycling stability. Specifically, VE increases by 7.1% at 80 mA cm^{-2} when the temperature is raised from 30 to 70 °C, primarily due to reduced polarization resulting from enhanced reaction kinetics and mass transport. In contrast, CE decreases as a result of increased bromine crossover and side reactions. Interestingly, the maximum operable areal capacity remains unaffected by temperature, while the ZBFB exhibits the best cycling stability when operated at 50 °C. Both *in situ* imaging and *ex situ* characterizations were performed to unravel the temperature-dependent behaviors responsible for these performance variations, providing mechanistic insights that guide the design and thermal management of high-performance ZBFB systems.

2. Experimental section and methods

2.1. Materials

Graphite felts (GFs) were purchased from Fuel Cell Store. Carbon paper was purchased from Toray industries, Inc. Zinc bromide ($ZnBr_2$, 98%), potassium chloride (KCl, 99.5%), and 1-ethyl-1-methylpyrrolidinium bromide (MEPBr, 99%) were purchased from Aladdin. All chemicals were used without any further purification.

2.2. Characterizations

Material surface morphology was observed by the field emission scanning electron microscope (FE-SEM, Tescan MAIA3). Crystal phases were characterized by X-ray diffraction patterns, which were obtained by the X-ray diffractometer (XRD, Rigaku SmartLab) with Cu K_β radiation at 45 kV. The composition and chemical state of electrodes before and after cycling were determined by X-ray photoelectron spectroscopy (XPS, K-Alpha, Thermo Scientific). The membrane surface morphology was observed by optical microscope (OM, OLYMPUS SZX7) equipped with a digital camera, 3D laser scanning microscope (KEYENCE VK-X200). The concentration of bromine species was detected by ultraviolet-visible (UV–Vis) spectrophotometer (754PC, Shanghai Jinghua Technology Instrument Co., Ltd.).

2.3. In situ monitoring cell and H-cell diffusion test

To *in situ* monitor the polybromide oil dynamics under different temperatures, a unique electrochemical cell as shown in Fig. S1 was devised using a glass plate as the substrate. Zinc foil and carbon paper served as the negative and positive electrodes, respectively, with an active area of 5 mm × 5 mm and a spacing of 3 mm. Copper foil was employed as the current collector. The chamber (13 mm × 13 mm × 10 mm) was filled with electrolyte (2 M $ZnBr_2$ + 3 M KCl + 0.4 M MEPBr) with a volume of ~1.7 mL. A coverslip (15 mm × 15 mm) was placed on top to provide an optical window and minimize water evaporation. Temperature was controlled by a heating stage and monitored with a thermocouple positioned near the observation area. Illumination was provided from above by LED lights. The cell was charged and discharged at a current density of 40 mA cm^{-2}. Images and videos were recorded through the coverslip using an optical camera. Bromine diffusion tests were conducted using a two-compartment H-cell separated by a porous polyolefin membrane. The left side was filled with fully charged catholyte containing polybromide species, while the right side contained the corresponding anolyte.

2.4. Electrochemical measurements

Cyclic voltammetry (CV), electrochemical impedance spectroscopy (EIS), linear sweep voltammetry (LSV), and Tafel measurements were conducted in a typical three-electrode cell on a SP-300 BioLogic electrochemical workstation. In the CV and EIS test, the GF (1 cm^2), Pt foil, and Ag/AgCl electrode were used as the working electrode (WE), counter electrode (CE), and reference electrode (RE), respectively. The solution for CV and EIS analysis was 0.05 M $ZnBr_2$ + 1 M KCl + 0.01 M MEPBr. CV was scanned from 0 to 1 V and 0 to −1.2 V (*vs.* Ag/AgCl) with a scan rate of 20 mV s^{-1} for positive and negative redox reactions, respectively. The frequency range of EIS test was 10^5 to 10^{-1} Hz. Tafel plots were measured with a porous electrode deposited with zinc as the WE, a zinc foil as the CE, and Ag/AgCl as the RE at a scan rate of 5 mV s^{-1} in a range of ±0.25 V *vs.* open circuit potential. LSV measurements for hydrogen evolution reaction (HER) were conducted at a scan rate of 5 mV s^{-1} in 3 M KCl electrolyte to avoid interference from zinc deposition. GF, Pt foil, and Ag/AgCl were employed as WE, CE, and RE, respectively. The charge-discharge curves of ZBFBs were recorded using a NEWARE battery test system. The ZBFBs were assembled by sandwiching a porous separator (~730 μm) between two 3.1 mm-thick GFs (2 cm × 2 cm) as both positive and negative electrodes. Solutions (15 mL) containing 2 M $ZnBr_2$ + 3 M KCl + 0.4 M MEPBr were employed as both positive and negative electrolytes and circulated through the electrochemical cell at a flow rate of 28 mL min^{-1} (30 rpm) using peristaltic pumps.

3. Results and discussion

We first examined the impacts of temperature on the rate

performance by operating ZBFBs at increasing current densities under different temperatures at a fixed areal capacity of 20 mAh cm^{-2}. As shown in Fig. 1a, at 30 °C, VE is the lowest across the entire current-density range and declines steadily with increasing current density. ZBFBs can stably operate only up to 240 mA cm^{-2}. When the current density is raised to 280 mA cm^{-2}, the voltage rapidly reaches a cut-off value of 2.5 V due to excessive polarization, rendering the battery inoperable (Fig. S2). When the temperature increases to 40 °C, a modest improvement in VE is observed, indicating partial mitigation of polarization loss. At 50 °C, VE improves further, especially at medium-to-high current densities. At 60 °C, the cell maintains relatively high VEs over the full current-density range. Finally, at 70 °C, the highest VEs are achieved at all tested current densities, indicating the strongest temperature-enhanced kinetics. However, further increasing the temperature to 80 and 90 °C leads to a slight decline in the maximum operating current density (Fig. S3), possibly due to more severe side reactions under these high temperatures. In addition, rising temperature is found to alleviate the fluctuation of CE, which becomes stable at 70 °C in Fig. 1b. The observed CE fluctuation results from the complex two-phase flow caused by the formation of the polybromide oily phase during the charging process, which will be discussed in detail in the following section. In addition, the average CE remains nearly constant from 30 to 50 °C (~97%) but decreases gradually above 60 °C in Fig. S4, indicating that elevated temperatures accelerate bromine crossover and parasitic side reactions. In contrast, the applied current density mainly affects polarization and thus has a stronger influence on VEs than on CEs. Energy efficiencies (EEs, defined as the product of VE and CE) show a similar trend as VEs (Fig. S5).

Fig. 1c displays the charge-discharge voltage profiles of ZBFBs operated at a typical current density of 80 mA cm^{-2}. As can be seen, raising the temperature from 30 to 70 °C reduces the charge voltage plateaus and increases the discharge voltage plateaus, thereby increasing VE from 76.6% at 30 °C to 83.7% at 70 °C (Fig. 1d). The improvement can be attributed to the enhanced reaction kinetics,

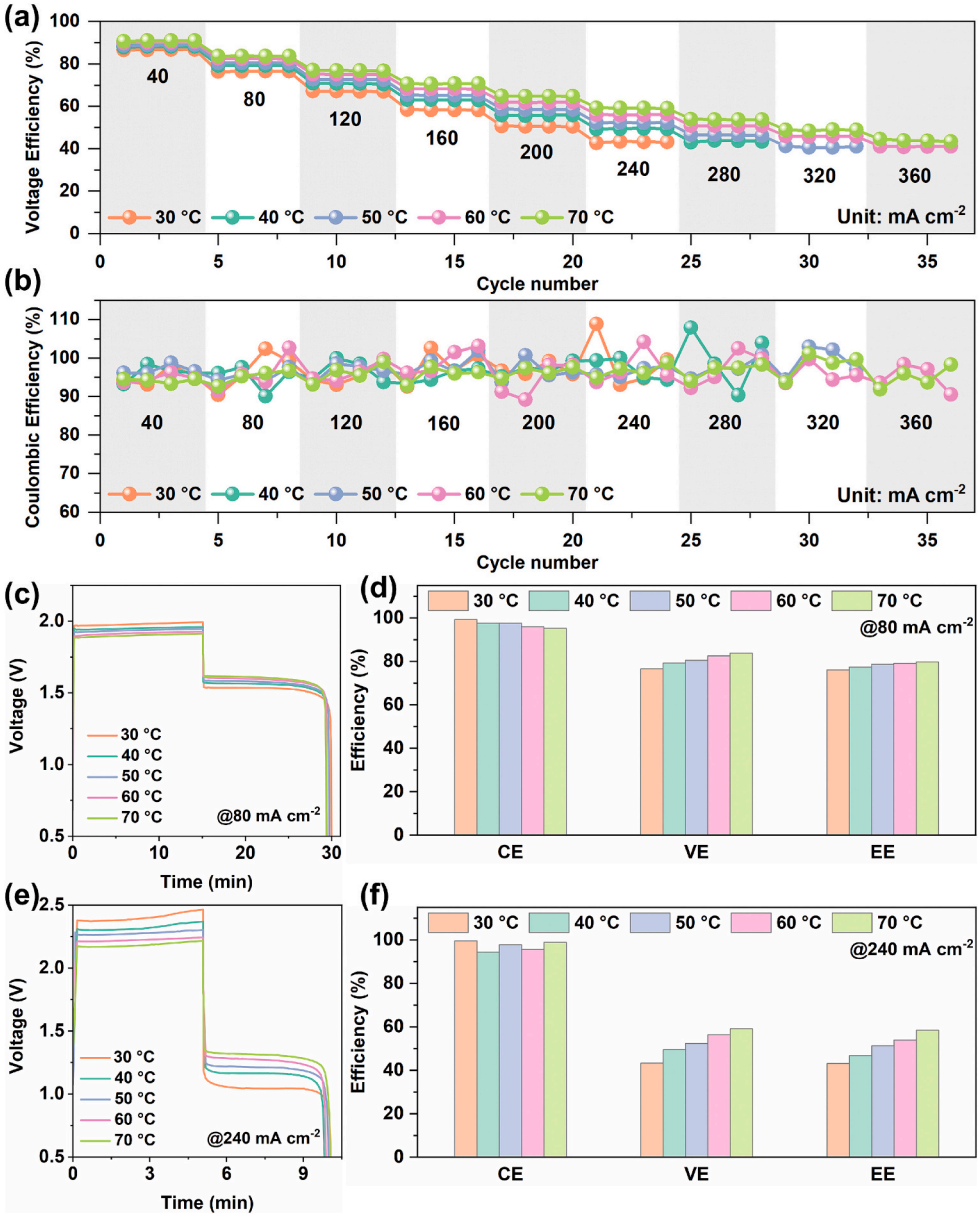

Fig. 1. (a) VEs and (b) CEs of ZBFBs at different temperatures when charged and discharged at various current densities. (c) Charge-discharge voltage profiles and (d) corresponding CEs, VEs, and EEs of ZBFBs at 80 mA cm^{-2} under different temperatures. (e) Charge-discharge voltage profiles and (f) corresponding CEs, VEs, and EEs of ZBFBs at 240 mA cm^{-2} under different temperatures.

increased electrolyte conductivity, and reduced electrolyte viscosity at higher temperatures, which alleviate activation, ohmic, and concentration polarizations. However, CE gradually declines as temperature increases, from 99.3% at 30 °C to 95.3% at 70 °C. To clarify the origin of CE decay, UV–Vis analysis of the charged catholyte was performed, and bromine crossover was evaluated by H-cell permeation tests. As shown in Fig. S6, the absorption intensity in the 260–280 nm region attributed to bromine and polybromide ions increases as the temperature increases, indicating that the concentration of bromine species increases in aqueous electrolyte from 30 to 70 °C, which is consistent with weakened bromine complexation and enhanced bromine mobility. The increased availability of these species in the electrolyte directly facilitates bromine crossover at higher temperatures. The H-cell images in Fig. S7 show progressively faster bromine transfer with increasing temperature, supporting that the reduced CE at elevated temperature is closely associated with intensified bromine crossover and self-discharge. Moreover, parasitic side reactions such as the HER and zinc corrosion may be intensified at higher temperatures, which also contribute to the reduced CEs [29]. The EEs show the same growth trend as VEs, but with a smaller magnitude due to the opposing trend in CE. When operated at a high current density of 240 mA cm^{-2}, the effects of temperature on charge-discharge process become more significant. As shown in Fig. 1e, the charge voltage is reduced from 2.39 to 2.18 V while the discharge voltage is increased from 1.05 to 1.31 V when the temperature is increased from 30 to 70 °C, leading to a much higher VE (Fig. 1f). Due to the short operating duration at this high current density, the CEs remain relatively stable under different temperatures. As a result, EEs display the same trend as VEs when temperature increases.

As a hybrid flow battery, the capacity and cycle life of ZBFBs are highly dependent on the amount and quality of deposited zinc. To determine the effects of temperature on areal capacity, we cycled the ZBFBs at a constant current density of 80 mA cm^{-2} with progressively

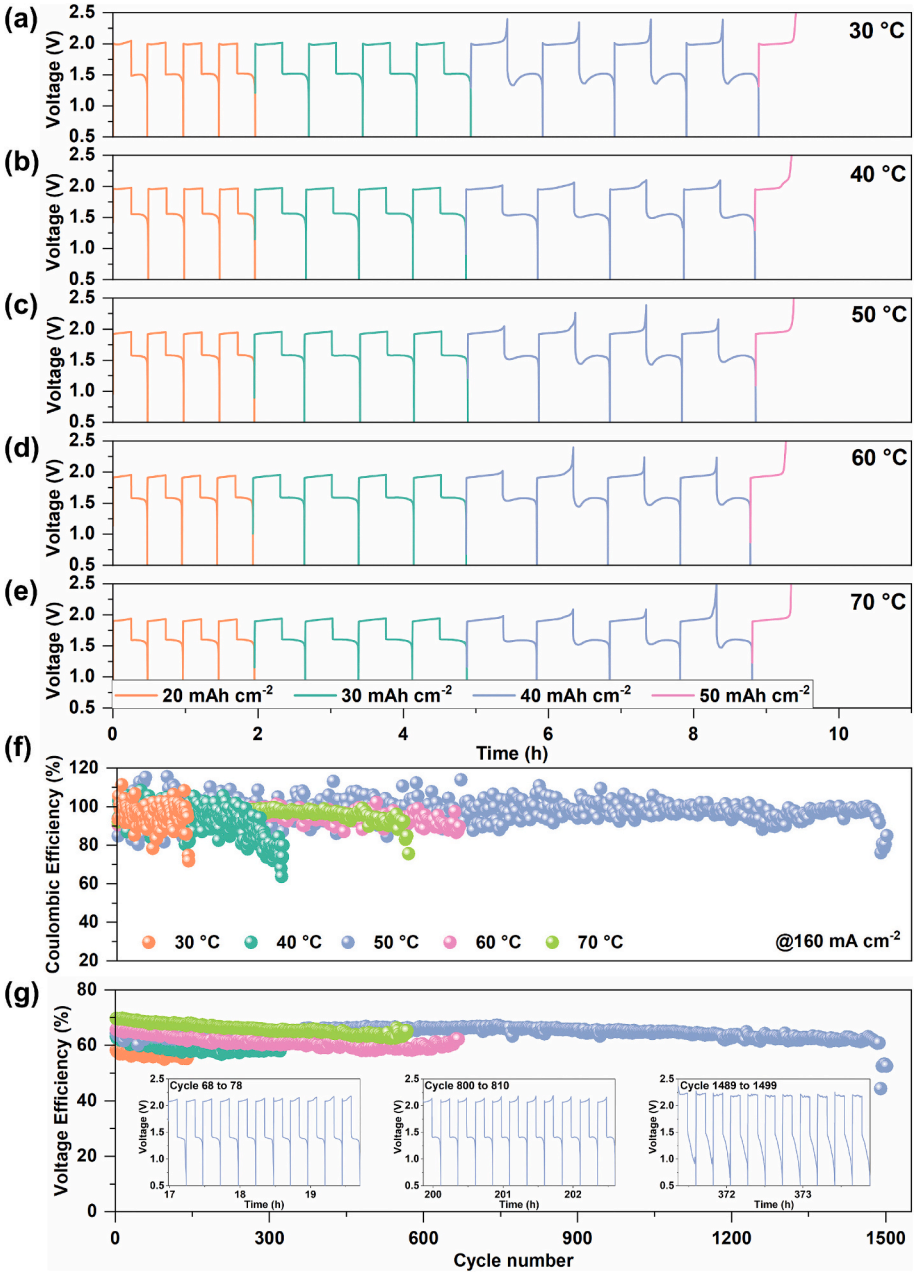

Fig. 2. Voltage-time curves of ZBFBs with increasing areal capacity at a constant current density of 80 mA cm^{-2} and (a) 30, (b) 40, (c) 50, (d) 60, and (e) 70 °C. (f) CEs and (g) VEs of ZBFBs cycled at 160 mA cm^{-2} and 20 mAh cm^{-2}. Insets in (g) show representative charge-discharge voltage curves at 50 °C.

increasing areal capacities. Fig. 2a-e present the charge and discharge voltage profiles at different temperatures (30–70 °C). Similar to the rate-performance results, as temperature increases, the voltage gap between the charge and discharge plateaus narrows under various areal capacities. Interestingly, it was found that at a relatively low areal capacity (*e.g.*, 20 and 30 mAh cm^{-2}), the charging voltage plateaus remain flat. However, when the areal capacity is increased to 40 mAh cm^{-2}, the voltages at the end of charging rise rapidly, indicating large concentration polarization. Attempts to operate ZBFBs at 50 mAh cm^{-2} failed as the charge voltage reached the cutoff voltage (2.5 V) and the charging process was terminated. This is because during the charging process, zinc tends to deposit on the electrode near the membrane side due to the shortest ion transport distance. As deposition continues, the electrodeposits gradually fill the pores, leading to increased transport resistance and eventually blocking the transport pathways. These phenomena occur at all tested temperatures, suggesting that raising temperature does not increase the maximum areal capacity of ZBFBs. Nevertheless, further increasing the operating temperature to 80 and 90 °C reduces the maximum areal capacity as shown in Fig. S8. This is possibly due to dramatically intensified side reactions and dendrite growth at these high temperatures. These results underscore the importance of thermal management for future ZBFBs to ensure reliable and durable operation.

Fig. 2f compares the cycling stability of ZBFBs at various temperatures at a current density of 160 mA cm^{-2} and an areal capacity of 20 mAh cm^{-2}. It is found that the cycle life decreases in the order of 50 °C > 60 °C > 70 °C > 40 °C > 30 °C. Moreover, the CEs vary more significantly at relatively low temperatures (30 and 40 °C). This is attributed to the complexation between generated elemental bromine and the bromine complexing agent (BCA), which leads to the formation of a denser polybromide oily phase during charging. Due to the poor mixing of the oily phase with the aqueous solution, some polybromides may not be efficiently reduced back during discharge, resulting in a low CE. Combined with the residual polybromides, more bromine species may participate in the following discharge process, leading to a much higher CE. These processes may be repeated during cycles, causing continuous fluctuations in CEs. Similar phenomena have been reported in previous works [25,30,31]. These fluctuations will exacerbate the unevenness of zinc deposition and dissolution, significantly reducing the cycle life of ZBFBs. Elevating the operating temperature alleviates the fluctuations of CE, probably due to the improved mixing of polybromide as a result of weakened complexation. Consequently, the cycle stability of ZBFBs increases as temperature rises during the initial stage, exceeding 1000 cycles at 50 °C. Further increasing the temperature to 60 and 70 °C adversely shortens the cycle life. This is because at higher temperatures, side reactions such as HER become significant, which alter the zinc deposit morphology and promote severe dendrite growth (details will be discussed in the following section), resulting in a shortened cycle life. In addition, it should be noted that although in the initial stage of the cycling process, higher temperatures lead to higher VEs (Fig. 2g), these positive effects gradually diminish as the cycle progresses (Fig. S9) and the decay rate of efficiency is accelerated at higher temperatures. SEM characterization of the post-cycling electrodes after 1000 cycles at 50 °C was conducted. As shown in Fig. S10, the electrode surfaces after cycling remain relatively intact, with no catastrophic structural damage observed, although minor changes are present compared to the fresh electrode. To further verify the interfacial evolution of the electrode, XPS measurements were performed on the positive electrode before and after cycling at different temperatures (Fig. S11). Full XPS spectra show that the peak intensity of O 1 s increases significantly with increasing temperature and remains higher after cycling compared to the pristine electrode. More importantly, the C 1 s spectra reveal the evolution of oxygen-containing carbon species, including C−O, C═O, and O−C=O components, while the corresponding O 1 s spectra show enhanced contributions from C−O/C−OH-related species after cycling. These changes become more evident at elevated temperatures, indicating that the positive electrode undergoes progressive surface oxidation during operation, which is consistent with the deterioration in cycling performance of ZBFBs [17]. For these reasons, the ZBFBs exhibit poor cycling performance at 80 and 90 °C as shown in Fig. S12, making them impractical for real-world applications. Therefore, these two temperatures were excluded from subsequent mechanistic analyses.

Unlike all soluble RFBs, ZBFBs feature the formation/dissolution of the oily phase and plating/stripping of zinc metal at the positive and negative electrodes, both of which possess their own temperature-dependent characteristics. Therefore, a series of characterizations were performed to unravel the underlying mechanisms governing the overall battery performance described above. CV tests were first conducted to evaluate the Br_2/Br^- reaction kinetics at different temperatures. As depicted in Fig. 3a, both the cathodic peak current and anodic current exhibit an increasing trend with rising temperature, indicating faster charge transfer kinetics and higher diffusivity of bromine species at elevated temperatures. Moreover, the cathodic peak potential shifts positively at higher temperatures, suggesting improved reversibility of the Br_2/Br^- redox process. In addition, EIS tests were performed to further analyze the electrochemical processes. Nyquist plots in Fig. S13 reveal that the semicircle radius decreases with increasing temperatures, indicating decreased charge transfer resistance for Br_2/Br^- reaction at elevated temperatures. The kinetic parameters calculated at different temperatures are summarized in Table S1 [32]. For the bromine reaction, j_0 increases from 2.62×10^{-4} to 6.79×10^{-4} A cm^{-2} and k_0 increases from 2.47×10^{-8} to 6.39×10^{-8} cm s^{-1} as temperature increases from 30 to 70 °C. CV tests at various scan rates were also conducted to calculate the diffusion coefficient as shown in Fig. S14 [33]. The diffusion coefficient increases markedly with temperature from 2.33×10^{-7} cm^2 s^{-1} (30 °C) to 8.71×10^{-7} cm^2 s^{-1} (50 °C) and 3.94×10^{-6} cm^2 s^{-1} (70 °C). This trend demonstrates substantially enhanced electrochemical response and faster mass transfer behavior at higher temperatures. These results are consistent with the improved VEs in full-cell performance tests.

To visualize the dynamics of the polybromide phase, an *in situ* monitoring platform was developed to investigate the evolution of polybromide droplets at various temperatures [34]. Fig. 3b and Video S1 display the dynamic behavior of the polybromide phase on a carbon paper during the charging process at three representative temperatures (30, 50, and 70 °C). At 30 °C, small red polybromide droplets nucleate at multiple sites, gradually grow, and eventually coalesce into larger droplets. At 50 °C, droplet formation is retarded, and the number of droplets on the carbon paper surface decreases significantly after 10 min of charging, due to the increased solubility of polybromide in the electrolyte. As charging proceeds, these droplets merge into a larger and more widely spread phase due to the decrease in surface tension at elevated temperatures [35]. The formation of the polybromide phase is further retarded at 70 °C, with only a few dispersed droplets formed at the end of the charging process. In addition, gas bubbles are formed and adhere to the surface of the carbon paper. These results demonstrate that the complexation effect of the BCA is greatly weakened while side reactions are triggered at this high temperature. The generation of bubbles may result from oxygen and/or chlorine evolution reactions due to enhanced kinetics at high temperatures, which may also be one of the reasons why the lifespan of ZBFBs is shortened under these conditions. The polybromide dynamics during the discharging process are presented in Fig. 3c and Video S2. As discharge proceeds, the droplets gradually dissolve as polybromides are reduced back to bromide ions. However, it is found that small residual droplets are left even at the end of discharge at 30 °C, indicating the sluggish polybromide dissolution kinetics, which is consistent with the CE fluctuations during battery operation. This result also underscores the importance of good mixing between polybromide and the aqueous electrolyte to ensure smooth operation of ZBFBs. By contrast, the entire polybromide floc shrinks uniformly and completely disappears at the end of discharge at 50 °C, indicating the efficient conversion of polybromide to bromide, which is driven by

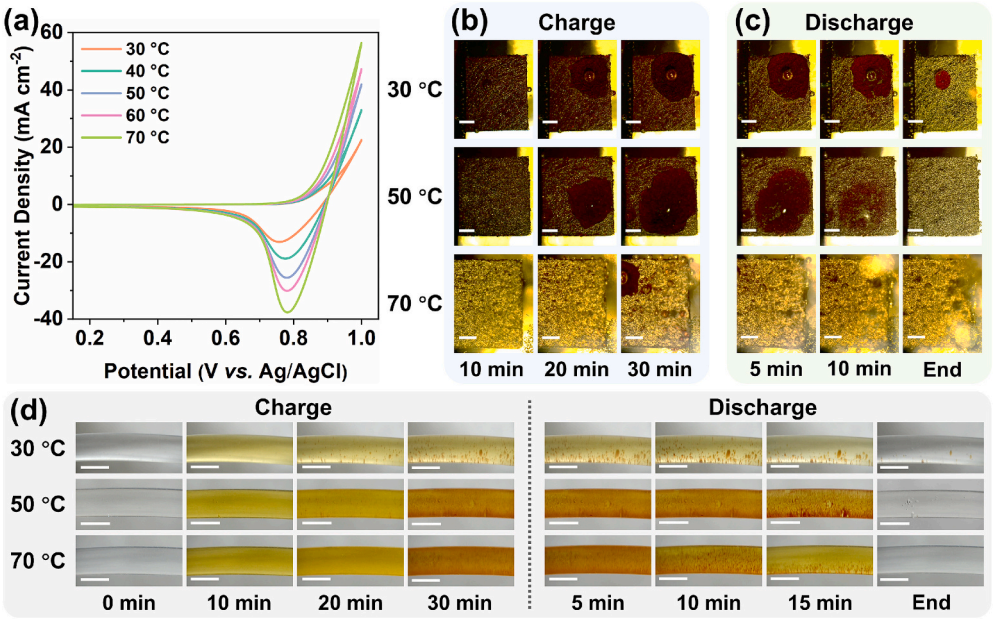

Fig. 3. (a) CV profiles of the Br_2/Br^- redox reaction at different temperatures with potential ranging from 0 to 1 V *vs.* Ag/AgCl. *In situ* monitoring images of polybromide droplets on carbon paper (5 mm × 5 mm) captured by an optical camera: (b) formation during the charging process and (c) dissolution during the discharging process (Scale bar: 1 mm). (d) *In situ* monitoring images of the positive electrolyte at the outlet of ZBFBs during the first cycle at a current density of 40 mA cm^{-2} (Scale bar: 4 mm).

enhanced bromine dissolution kinetics at this moderate temperature. This is because increasing temperature reduces the viscosity of the electrolyte and improves the diffusivity of bromine and polybromide species, facilitating their transport and reactivity at the interface. In addition, the interfacial tension between polybromide droplets and the bulk electrolyte is lower, which helps to reduce the residual oily phase and enhance the dissolution rate. At 70 °C, as only a few oily phases are formed, they completely dissolve during discharge. A large fraction of bromine exists as free or weakly complexed bromine which continues to diffuse and react with the zinc electrodes, resulting in severe self-discharge and thus the shortest discharge time at the same current density.

In addition, the color variations of the positive electrolyte at the outlet of ZBFBs during the first cycle were recorded, which also serve as a visual representation of the amount and stability of bromine and the polybromide complex leaving the electrode. As shown in Fig. 3d, after charging for 10 min, the color of aqueous electrolyte gradually deepens as the temperature rises due to the increased solubility of bromine in the electrolyte. After the complex droplets appear, which indicates the saturation of bromine, the color of the aqueous phase remains almost unchanged. At 30 °C, numerous near-spherical complex droplets appear at the early stage of charging, and the color remains the lightest due to the strong complexation effect and the low solubility of the oily phase droplets in the electrolyte. At 50 °C, the shape of the complex droplets becomes irregular, but numerous droplets are still observed at the outlet at the end of charge, demonstrating that the BCA is still effectively complexing the generated bromine. At the end of charging at 70 °C, due to the deterioration of BCA complexation and the decrease in surface tension, almost no large droplet formation was observed, and the complex phase shows a more uniform mist-like distribution in the entire aqueous electrolyte. These trends are consistent with previous *in situ* studies showing that BCA forms dense polybromide droplets whose amount and interfacial behavior are strongly dependent on temperature [36]. During discharge, the color of electrolyte at the outlet gradually lightens as bromine is reduced back to bromide ions. Notably, it is clearly observed that even though the aqueous electrolyte becomes transparent at the end of discharge, some small droplets remain at 30 °C, indicating a slow decomplexation rate and poor mixing with the aqueous electrolyte. As mentioned before, this is the root cause of the fluctuation of CEs during cycling and possibly a key contributor to the non-uniform zinc deposition. During the 15-min discharge, no significant color change in the electrolyte was observed at 50 and 70 °C. This is because the dissolution rate of droplets accelerates at elevated temperatures, maintaining a higher bromine concentration in the aqueous phase. Then the electrolyte becomes transparent again with no residual droplets by the end of discharge, indicating the efficient conversion of polybromide back to bromide, which also explains the relatively stable CEs in battery performance tests. In addition, temperature may also influence the effectiveness of BCAs. As temperature increases, the complexation equilibrium and bromine phase distribution can shift, potentially reducing the ability of the BCA to immobilize bromine. This would increase the activity of dissolved bromine species and contribute to enhanced crossover and self-discharge at elevated temperatures.

While the preceding results show that increasing temperature does not affect the areal capacity of ZBFBs, which corresponds to the total amount of zinc deposited on the negative electrode, operating temperature has been reported to have a profound effect on zinc deposition behavior in static cells [37,38]. Thus, a series of characterizations were conducted to examine the effects of temperature on the electrochemical performance of the zinc electrode in ZBFBs. CV tests were performed to evaluate the zinc deposition/dissolution behavior at different temperatures. As shown in Fig. 4a, the initial zinc deposition potential shifts positively with increasing temperature, indicating a reduced nucleation overpotential. More specifically, the nucleation overpotential is reduced from 39.6 mV at 30 °C to 15.7 mV at 70 °C, indicating a smaller barrier for zinc deposition, which is beneficial for the uniform deposition of zinc [28]. Moreover, as the temperature increases, the anodic peak currents and cathodic currents gradually increase, indicating the enhanced reaction kinetics and mass transport [39]. Nyquist plots show that the semicircle diameter decreases markedly with increasing temperatures, indicating reduced charge transfer resistance at elevated temperature (Fig. S15). It was calculated that j_0 for Zn^{2+}/Zn redox reaction increases from 0.30×10^{-4} to 3.34×10^{-4} A cm^{-2} and k_0 increases from 0.31×10^{-8} to 3.47×10^{-8} cm s^{-1} (Table S1). This trend is especially pronounced compared to that of the Br_2/Br^- reaction, suggesting that the negative electrode kinetics are more sensitive to temperature variations

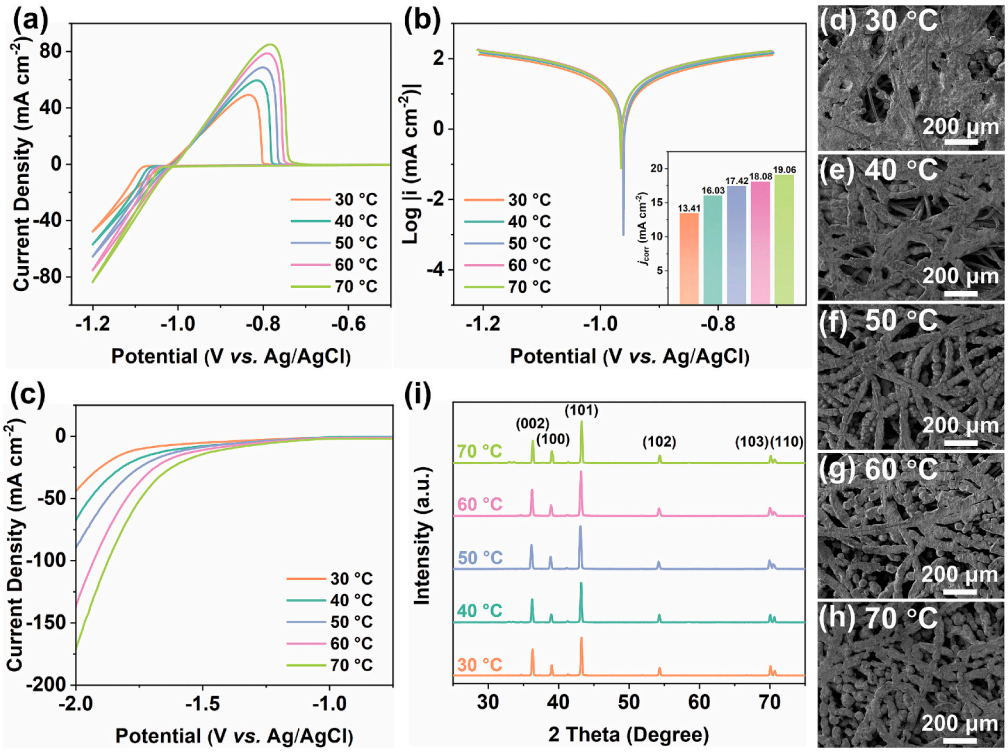

Fig. 4. (a) CV profiles at different temperatures over a potential range of −1.2 to −0.5 V *vs.* Ag/AgCl. (Due to the low current response, CV curves in the range of −0.5 to 0 V are omitted for clearer comparison and the complete CV curves are shown in Fig. S19) (b) Tafel plots of zinc-deposited anodes at different temperatures, with an inset showing the corresponding calculated corrosion current densities. (c) LSV curves for HER in 3 M KCl electrolytes at 5 mV s^{-1} and different temperatures. (d-h) SEM images of deposited zinc at an areal capacity of 20 mAh cm^{-2} and different temperatures. (i) XRD patterns of deposited zinc on GFs at 80 mA cm^{-2} for 15 min and different temperatures.

than those of the positive electrode [33,40]. Since the zinc electrode is thermodynamically unstable in aqueous solution, it is expected that increasing temperature will exacerbate side reactions. To quantify the corrosion rate at various temperatures, the Tafel test was carried out. As shown in Fig. 4b, the corrosion current density acquired from Tafel plots increases from 13.41 mA cm^{-2} at 30 °C to 19.06 mA cm^{-2} at 70 °C, confirming the accelerated zinc corrosion at high temperatures. Additionally, LSV measurements were conducted in 3 M KCl solution (to exclude the interference of zinc deposition) to investigate the temperature effect on HER. Fig. 4c shows that as the temperature increases, the onset potential of HER shifts positively and the current density associated with HER increases significantly, due to the enhanced activity for water decomposition reaction at elevated temperatures [28]. It should be noted that HER is a detrimental side reaction for the stable operation of ZBFBs, as it not only consumes protons and thus increases the pH value, which causes the precipitation of insulating products, but also generates hydrogen bubbles that disrupt the ion transport pathway and trigger severe dendrite growth as shown in Fig. S16 [41]. Therefore, further work should also focus on suppressing HER over a wide temperature range.

Morphology and distribution of zinc deposits on the electrodes were also observed by SEM after being charged at 80 mA cm^{-2} for 15 min (corresponding to 20 mAh cm^{-2}) at different temperatures. As displayed in Fig. 4d, electrode fibers are partially covered with zinc deposits at 30 °C, which consist of dense lamellar flakes at high magnification (Fig. S17). This microstructure arises from low nucleation density and basal plane growth [28]. As the temperature rises to 40 °C, zinc deposition coverage improves as shown in Fig. 4e. This is because the nucleation sites increase with the decrease of nucleation overpotential and the improvement of mass transport. At 50 °C, the nucleation sites continue to increase, resulting in the formation of larger zinc particles that uniformly cover the fiber surface with a moderate porosity, which is favorable for reversible Zn plating/stripping, so that the ZBFB can achieve the longest cycle life (Fig. 4f). At higher temperatures, severe HER produces bubbles that adhere to the electrode surface, also adversely affecting the zinc deposition uniformity as depicted in Fig. 4g and h. The zinc deposits at 70 °C exhibit larger granularity, and these loosely connected zinc particles are prone to partial detachment during the stripping process, suggesting increased roughness and resulting in the formation of dead zinc during long-term cycling [39,42]. These qualitative structural differences are consistent with the observed temperature-dependent cycling stability. More importantly, the morphology evolution suggests that 50 °C provides the best balance between deposition kinetics and growth stability, rather than fully suppressing dendrite formation. It should be noted that temperature primarily affects deposit uniformity and compactness, rather than introducing a binary transition between dendritic and non-dendritic growth. In order to determine the crystal structure at different temperatures, XRD measurements were carried out and the results are shown in Fig. 4i. The intensity of all peaks is normalized with respect to the (102) plane. As temperature increases, the intensity of the (002) peak decreases, while the (101) and (100) peaks intensify, which is consistent with the morphology observed by SEM. Previous studies have reported that the (002) plane possesses the lowest thermodynamic free energy compared to other crystal planes, rendering it the primary surface for zinc deposition at low temperatures [43,44]. As temperature increases, other planes gain opportunities to participate in deposition, leading to a weakening of the (002) peak intensity [21]. When (100) and (101) crystal planes dominate, the deposited zinc tends to grow at larger angles relative to the substrate [45]. Moreover, coupled with severe side reactions at elevated temperatures, these factors typically result in the formation of coarse zinc deposits that can puncture the membrane and cause short circuits in ZBFBs. XRD characterization was also performed to further evaluate the corrosion-related products on the zinc-deposited

electrode after cycling at different temperatures. As shown in Fig. S18, in addition to the characteristic diffraction peaks of metallic zinc, weak additional peaks corresponding to $Zn_5(OH)_8Cl_2{\cdot}H_2O$ (PDF#07–0155) are observed, indicating the formation of a chloride-containing corrosion product on the zinc deposited electrode. Notably, these peaks become more pronounced at 70 °C, while no new phases are detected. This observation suggests that elevated temperatures accelerate the formation of corrosion products without altering the underlying corrosion mechanism.

Ion diffusion behavior across the membrane was studied by measuring the transmembrane resistance at different temperatures. Fig. S20 compares the resistance with/without the membrane, showing that resistance decreases as temperature rises due to reduced viscosity and increased ionic conductivity [46]. The reduction in resistance is more pronounced in the presence of the porous separator. This is understandable because ion transport in the separator is more restricted by narrow pores, while heating significantly alleviates these limitations by increasing ion mobility and slightly expanding the membrane structure [47,48]. The calculation results show that the lowest transmembrane resistance occurs at 70 °C (Fig. 5a), enabling the highest VE for ZBFBs. However, the reduction levels off after 50 °C, probably because ionic mobility and membrane structural changes approach their limits. Finally, the self-discharge performance was assessed by resting the battery for six hours after charging, followed by discharging to a cutoff voltage of 0.5 V. The resulting voltage-time profiles are shown in Fig. 5b. During the resting period, the open-circuit voltage remains relatively stable. Although ZBFBs at higher temperatures exhibit higher initial discharge voltages, they deliver significantly lower discharge capacities. As shown in Fig. 5c, the capacity retention rate is dramatically reduced from 83.12% to 54.28% as the temperature rises from 30 to 70 °C, indicating exacerbated self-discharge at elevated temperatures. The decline becomes particularly pronounced at 60 and 70 °C, which can be attributed to several factors. First, heating accelerates the diffusion and transport of bromine and polybromide from the positive to the negative electrolyte, leading to severe bromine crossover and thus self-discharge [25,49]. Second, the reduced capability of the BCA to complex bromine at high temperatures results in more free or weakly bound bromine in the electrolyte, further promoting bromine crossover [36]. In addition, high temperatures enhance side reactions, such as chemical corrosion of zinc by bromine and HER, further reducing the discharge capacity [39]. After long-term operation at 70 °C, the post-cycled membrane exhibits a noticeably rough surface compared to the pristine one. However, no macroscopic rupture or catastrophic failure is observed (Fig. S21a-c). Despite the absence of visible mechanical failure, the bromine permeation rate through the post-cycled membrane is significantly faster than the fresh membrane as shown in Fig. S21d and e, indicating deterioration of its bromine-blocking capability. Therefore, the increased self-discharge at elevated temperature is attributed to the combined effects of weakened bromine complexation and aggravated bromine crossover as a result of separator aging. These findings suggest that ZBFBs using MEPBr as the BCA are unsuitable for operation above 50 °C. Future work should focus on developing effective thermal management strategies or advanced BCAs to expand the thermal adaptability of ZBFBs.

4. Conclusions

In summary, a systematic investigation into the impact of operating temperature on the performance of ZBFBs and the underlying temperature-dependent electrochemical behavior was conducted. Our results demonstrate that temperature plays a crucial role in governing the electrochemical processes in ZBFBs. Increasing the temperature effectively reduces polarization, narrows the charge-discharge voltage gap, and thus improves VE, but decreases CE due to enhanced bromine crossover and side reactions. While areal capacity remains largely unaffected, cycling stability is highly temperature-dependent. *In situ* and *ex situ* analyses reveal that the battery performance is strongly linked to zinc deposit morphology and polybromide phase dynamics. The benefits of higher temperatures (improved VE, EE, and stability) diminish above 50 °C due to intensified dendrite growth, side reactions, and self-discharge. Operating ZBFBs near 50 °C achieves the best balance among fast reaction kinetics, effective bromine complexation/dissolution, and stable zinc reversibility, enabling over 1000 cycles at 160 mA cm^{-2}. While the trend and mechanistic insights in this study are broadly applicable, the precise optimal temperature may vary under different system conditions, such as electrolyte composition, bromine complexing agent, flow rate, membrane properties, electrode structure, and operating current density. Nevertheless, these findings still highlight for the first time the crucial role of temperature in regulating the performance of ZBFBs and provide a foundation for thermal management to facilitate their practical applications.

CRediT authorship contribution statement

Jiayi Li: Writing – review & editing, Writing – original draft, Visualization, Validation, Software, Methodology, Investigation, Formal analysis, Data curation, Conceptualization. **Wenjun Liu:** Writing – review & editing, Validation, Software, Investigation, Formal analysis, Data curation, Conceptualization. **Yongzi Chen:** Writing – review & editing, Validation, Investigation, Formal analysis, Data curation, Conceptualization. **Maochun Wu:** Writing – review & editing,

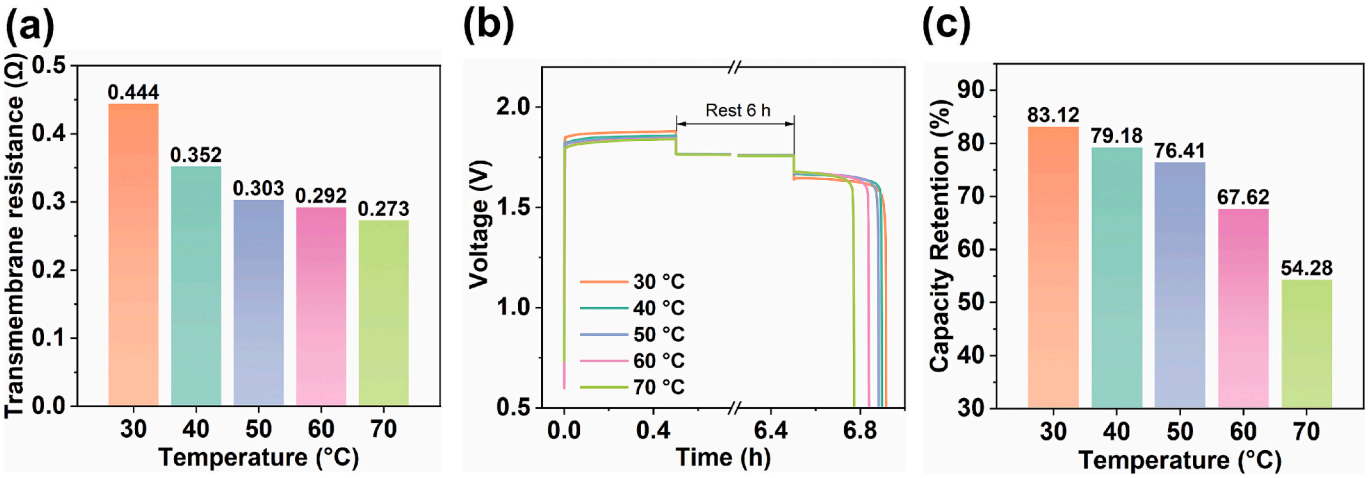

Fig. 5. (a) Transmembrane resistance at different temperatures. (b) Charge-rest-discharge voltage-time profiles and (c) corresponding capacity retention of ZBFBs at different temperatures.

Supervision, Resources, Project administration, Funding acquisition, Conceptualization.

Declaration of competing interest

The authors declare no conflict of interest.

Acknowledgment

The work described in this paper was fully supported by the grants from the Research Grants Council of the Hong Kong Special Administrative Region, China (Project No. 16205721 and 25232523).

Appendix A. Supplementary data

Supplementary data to this article can be found online at https://doi.org/10.1016/j.est.2026.122402.

Data availability

Data will be made available on request.

References

[1] Z. Li, Y.C. Lu, Material design of aqueous redox flow batteries: fundamental challenges and mitigation strategies, Adv. Mater. 32 (2020) 2002132, https://doi.org/10.1002/adma.202002132.
[2] T. Xiong, W.S.V. Lee, S.X. Dou, Designing high-performance direct photo-rechargeable aqueous Zn-based energy storage technologies, Carbon Neutrality 3 (2024) 28, https://doi.org/10.1007/s43979-024-00104-9.
[3] R. Wang, M. Hao, C. He, Z. Tu, F. Chong, Y. Li, Gradient-distributed NiCo2O4 nanorod electrode for redox flow batteries: establishing the ordered reaction interface to meet the anisotropic mass transport, Appl. Catal. B Environ. 332 (2023) 122773, https://doi.org/10.1016/j.apcatb.2023.122773.
[4] D. Xi, A.M. Alfaraidi, J. Gao, T. Cochard, L.C.I. Faria, Z. Yang, T.Y. George, T. Wang, R.G. Gordon, R.Y. Liu, M.J. Aziz, Mild pH-decoupling aqueous flow battery with practical pH recovery, Nat. Energy 9 (2024) 479–490, https://doi.org/10.1038/s41560-024-01474-1.
[5] J. Li, Z. Xu, M. Wu, Halogen enabled aqueous flow cells for large-scale energy storage : current status and perspectives, J. Power Sources 581 (2023) 233477, https://doi.org/10.1016/j.jpowsour.2023.233477.
[6] H. Iqbal, S. Sarwar, D. Kirli, J.K.H. Shek, A.E. Kiprakis, A survey of second-life batteries based on techno-economic perspective and applications-based analysis, Carbon Neutrality 2 (2023) 8, https://doi.org/10.1007/s43979-023-00049-5.
[7] J. Sun, Z. Guo, L. Pan, X. Fan, L. Wei, T. Zhao, Redox flow batteries and their stack-scale flow fields, Carbon Neutrality 2 (2023) 30, https://doi.org/10.1007/s43979-023-00072-6.
[8] L. Tang, W. Lu, H. Zhang, X. Li, Progress and perspective of the cathode materials towards bromine-based flow batteries, Energy Mater. Adv. 2022 (2022) 9850712, https://doi.org/10.34133/2022/9850712.
[9] M. Nakatsuji-Mather, T.K. Saha, Zinc-bromine flow batteries in residential electricity supply: two case studies, IEEE Power Energy Soc. Gen. Meet. (2012) 1–8, https://doi.org/10.1109/PESGM.2012.6344777.
[10] Y. Sera, T. Nakayama, 4 MW zinc-bromine battery for electric power storage, in: Energy Convers. Eng. Conf, 1989, pp. 1319–1323, https://doi.org/10.1109/IECEC.1989.74639.
[11] P. Eidler, Development of Zinc/Bromine Batteries for Load-Leveling Applications: Phase 1 Final Report, United States, 1999, https://doi.org/10.2172/9466.
[12] N.H. Clark, P. Eidler, Development of Zinc/Bromine Batteries for Load-Leveling Applications: Phase 2 Final Report, United States, 1999, https://doi.org/10.2172/14816.
[13] R. Wang, Y. Li, Carbon electrodes improving electrochemical activity and enhancing mass and charge transports in aqueous flow battery: status and perspective, Energy Storage Mater. 31 (2020) 230–251, https://doi.org/10.1016/j.ensm.2020.06.012.
[14] R. Wang, Bi-layer graphite felt as the positive electrode for zinc-bromine flow batteries: achieving efficient redox reaction and stable mass transport, J. Energy Storage 74 (2023) 109487, https://doi.org/10.1016/j.est.2023.109487.
[15] C. Zhang, T.S. Zhao, Q. Xu, L. An, G. Zhao, Effects of operating temperature on the performance of vanadium redox flow batteries, Appl. Energy 155 (2015) 349–353, https://doi.org/10.1016/j.apenergy.2015.06.002.
[16] X. Zhang, Y. Liu, S. Wang, J. Wang, F. Cheng, Y. Tong, L. Wei, Z. Fang, J. Mao, Fundamentals and design strategies of electrolytes for high-temperature zinc-ion batteries, Energy Storage Mater. 70 (2024) 103471, https://doi.org/10.1016/j.ensm.2024.103471.
[17] Z. Huang, Z. Xiao, Y. Luo, X. Xie, L. Tan, Y. Deng, J. Wu, Y. Liu, Y. Liu, F. Zhu, D. Li, G. Li, Operational temperature effects on redox flow batteries performance: a comprehensive review, J. Energy Storage 131 (2025) 117631, https://doi.org/10.1016/j.est.2025.117631.
[18] P. Rao, S. Jayanti, Influence of electrode design parameters on the performance of vanadium redox flow battery cells at low temperatures, J. Power Sources 482 (2021) 228988, https://doi.org/10.1016/j.jpowsour.2020.228988.
[19] P. Rao, S. Jayanti, Physics-based electrochemical model of vanadium redox flow battery for low-temperature applications, Batteries 9 (2023) 374, https://doi.org/10.3390/batteries9070374.
[20] J. Ren, Z. Wang, B. Liu, Q. Yue, X. Fan, T. Zhao, Thermal effects on the performance of stack-scale vanadium redox flow batteries, J. Electrochem. Soc. 170 (2023) 010539, https://doi.org/10.1149/1945-7111/acb4bc.
[21] Y. Cheng, H. Zhang, Q. Lai, X. Li, Q. Zheng, X. Xi, C. Ding, Effect of temperature on the performances and in situ polarization analysis of zinc-nickel single flow batteries, J. Power Sources 249 (2014) 435–439, https://doi.org/10.1016/j.jpowsour.2013.10.115.
[22] B.S. Jayathilake, E.J. Plichta, M.A. Hendrickson, S.R. Narayanan, Improvements to the coulombic efficiency of the Iron electrode for an all-iron redox-flow battery, J. Electrochem. Soc. 165 (2018) A1630–A1638, https://doi.org/10.1149/2.0451809jes.
[23] Z. Xu, M. Wu, Toward dendrite-free deposition in zinc-based flow batteries: status and prospects, Batteries 8 (2022) 117, https://doi.org/10.3390/batteries8090117.
[24] L. Tang, T. Li, W. Lu, X. Li, Lamella-like electrode with high Br 2 -entrapping capability and activity enabled by adsorption and spatial confinement effects for bromine- based flow battery, Sci. Bull. 67 (2022) 1362–1371, https://doi.org/10.1016/j.scib.2022.05.012.
[25] X. Li, T. Li, P. Xu, C. Xie, Y. Zhang, X. Li, A complexing agent to enable a wide-temperature range bromine-based flow battery for stationary energy storage, Adv. Funct. Mater. 31 (2021) 2100133, https://doi.org/10.1002/adfm.202100133.
[26] G. Lu, Z. Wang, S. Zhang, J. Ding, J. Luo, X. Liu, Cathode materials for halide-based aqueous redox flow batteries: recent progress and future perspectives, Nanoscale 15 (2023) 4250–4260, https://doi.org/10.1039/d2nr07291b.
[27] J. Su, X. Yin, H. Zhao, H. Yang, D. Yang, L. He, M. Wang, S. Jin, K. Zhao, Y. Wang, Y. Wei, Temperature-dependent nucleation and electrochemical performance of Zn metal anodes, Nano Lett. 22 (2022) 1549–1556, https://doi.org/10.1021/acs.nanolett.1c04353.
[28] X. Li, C. Yuan, X. Chen, Q. Fu, S. Wang, G. Zhang, C. Xie, X. Li, Q. Fu, Temperature-dependence of Zn deposition/stripping behavior in aqueous Zn-based flow batteries, J. Energy Chem. 107 (2025) 260–268, https://doi.org/10.1016/j.jechem.2025.03.049.
[29] Z. Xu, J. Li, M. Wu, A high-rate and long-life zinc-bromine flow battery, J. Power Sources 613 (2024) 234869, https://doi.org/10.1016/j.jpowsour.2024.234869.
[30] X. Li, C. Xie, T. Li, Y. Zhang, X. Li, Low-cost titanium–bromine flow battery with ultrahigh cycle stability for grid-scale energy storage, Adv. Mater. 32 (2020) 2005036, https://doi.org/10.1002/adma.202005036.
[31] Y. Hu, Z. Min, G. Zhu, Y. Zhang, Y. Pei, C. Chen, Y. Sun, G. Liang, H.M. Cheng, Predeposited lead nucleation sites enable a highly reversible zinc electrode for stable zinc-bromine flow batteries, Nat. Commun. 16 (2025) 3255, https://doi.org/10.1038/s41467-025-58473-3.
[32] Y. Vetriselvam, G.S. Ramachandran, R. Naresh, K. Mariyappan, R. Pitchai, M. Ulaganathan, Improved electro-kinetics of new electrolyte composition for realizing high-performance zinc-bromine redox flow battery, Next Energy 4 (2024) 100123, https://doi.org/10.1016/j.nxener.2024.100123.
[33] R. Wang, Y. Li, Y. Wang, Z. Fang, Phosphorus-doped graphite felt allowing stabilized electrochemical interface and hierarchical pore structure for redox flow battery, Appl. Energy 261 (2020) 114369, https://doi.org/10.1016/j.apenergy.2019.114369.
[34] C. Wang, Q. Xie, G. Wang, Y. Lyu, Q. Wang, X. Ma, H. Wang, T. Guo, Y. Wu, J. Han, Visualizing and understanding the ionic liquid-mediated polybromide electrochemistry for aqueous zinc-bromine redox batteries, Nano Lett. 24 (2024) 13796–13804, https://doi.org/10.1021/acs.nanolett.4c04167.
[35] S.C. Leach, C.M. Ablow, K. Kinoshita, Mathematical analysis of axisymmetric sessile drop: application to the reduction of bromine in a two-phase electrolyte, J. Colloid Interface Sci. 92 (1983) 489–498, https://doi.org/10.1016/0021-9797(83)90170-4.
[36] U. Jiménez-Blasco, J.C. Arrebola, A. Caballero, Recent advances in bromine complexing agents for zinc–bromine redox flow batteries, Materials (Basel) 16 (2023) 7482, https://doi.org/10.3390/ma16237482.
[37] Y. Zuo, K. Wang, P. Pei, M. Wei, X. Liu, Y. Xiao, P. Zhang, Zinc dendrite growth and inhibition strategies, Mater. Today Energy 20 (2021) 100692, https://doi.org/10.1016/j.mtener.2021.100692.
[38] K. Yan, J. Wang, S. Zhao, D. Zhou, B. Sun, Y. Cui, G. Wang, Temperature-dependent nucleation and growth of dendrite-free lithium metal anodes, Angew. Chem. 131 (2019) 11486–11490, https://doi.org/10.1002/ange.201905251.
[39] J. Chen, M. Zhu, M. Gan, X. Wang, C. Gu, J. Tu, Rapid electrodeposition and corrosion behavior of Zn coating from a designed deep eutectic solvent, Metals (Basel) 13 (2023) 172, https://doi.org/10.3390/met13010172.
[40] S. Zhang, X. Ma, H. Hong, Y. Hou, Z. Huang, Catalytic electrolytes enable fast reaction kinetics and temperature adaptability for aqueous zinc-bromine flow batteries, Nat. Commun. 16 (2023) 10097, https://doi.org/10.1038/s41467-025-65047-w.
[41] N.S. Alghamdi, M. Rana, X. Peng, Y. Huang, J. Lee, J. Hou, I.R. Gentle, L. Wang, B. Luo, Zinc–bromine rechargeable batteries: From device configuration, electrochemistry, material to performance evaluation, Nano-Micro Lett. 15 (2023) 209, https://doi.org/10.1007/s40820-023-01174-7.
[42] W. Lu, C. Xie, H. Zhang, X. Li, Inhibition of zinc dendrite growth in zinc-based batteries, ChemSusChem 11 (2018) 3996–4006, https://doi.org/10.1002/cssc.201801657.

[43] Y. Zhang, X. Han, R. Liu, Z. Yang, S. Zhang, Y. Zhang, H. Wang, Y. Cao, A. Chen, J. Sun, Manipulating the zinc deposition behavior in hexagonal patterns at the preferential Zn (100) crystal plane to construct surficial dendrite-free zinc metal anode, Small 18 (2022) 2105978, https://doi.org/10.1002/smll.202105978.
[44] S. Wang, Z. Wang, Y. Yin, T. Li, N. Chang, F. Fan, H. Zhang, X. Li, A highly reversible zinc deposition for flow batteries regulated by critical concentration induced nucleation, Energy Environ. Sci. 14 (2021) 4077–4084, https://doi.org/10.1039/d1ee00783a.
[45] J. Cao, D. Zhang, C. Gu, X. Wang, S. Wang, X. Zhang, J. Qin, Z. Wu, Manipulating crystallographic orientation of zinc deposition for dendrite-free zinc ion batteries, Adv. Energy Mater. 11 (2021) 2101299, https://doi.org/10.1002/aenm.202101299.
[46] G.J. Janz, F.W. Dampier, G.R. Lakshminarayanan, P.K. Lorenz, R.P.T. Tomkins, Molten Salts: Volume 1, Electrical Conductance, Density, and Viscosity Data, 1968.
[47] R. Kim, H.G. Kim, G. Doo, C. Choi, S. Kim, J.H. Lee, J. Heo, H.Y. Jung, H.T. Kim, Ultrathin Nafion-filled porous membrane for zinc/bromine redox flow batteries, Sci. Rep. 7 (2017) 10503, https://doi.org/10.1038/s41598-017-10850-9.
[48] J. Cai, T. Jin, J. Kou, S. Zou, J. Xiao, Q. Meng, Lucas-Washburn equation-based modeling of capillary-driven flow in porous systems, Langmuir 37 (2021) 1623–1636, https://doi.org/10.1021/acs.langmuir.0c03134.
[49] M. Rana, N. Alghamdi, X. Peng, Y. Huang, B. Wang, L. Wang, I.R. Gentle, S. Hickey, B. Luo, Scientific issues of zinc-bromine flow batteries and mitigation strategies, Exploration 3 (2023) 20220073, https://doi.org/10.1002/EXP.20220073.